https://doi.org/10.5194/nhess-2022-32
Preprint. Discussion started: 4 February 2022

Natural Hazards and Earth System Sciences
Open Access
EGU
Discussions

Delimiting rockfall runout zones using reach probability values simulated with a Monte-Carlo based 3D trajectory model

Luuk Dorren[1,11], Frédéric Berger[2,11], Franck Bourrier[2], Nicolas Eckert[2,3], Charalampos Saroglou[4], Massimiliano Schwarz[1,11], Markus Stoffel[5,6,7], Daniel Trappmann[8], Hans-Heini Utelli[9], and Christine Moos[1,10]

[1]Bern University of Applied Sciences BFH-HAFL, Länggasse 85, CH-3052 Zollikofen, Switzerland
[2]INRAE, Grenoble, France
[3]Université Grenoble Alpes, Grenoble, France
[4]School of Civ. Eng., Nat. Techn. Univ. Athens, Greece
[5]Climatic Change Impacts and Risks in the Anthropocene (C-CIA), Institute for Environmental Sciences, University of Geneva, Geneva, Switzerland
[6]Dendrolab.ch, Department of Earth Sciences, University of Geneva, Geneva, Switzerland
[7]Department of F.A. Forel for Environmental and Aquatic Sciences, University of Geneva, Geneva, Switzerland
[8]Bayerische Staatsforsten, Marquartstein, Germany
[9]Impuls AG, Thun, Switzerland
[10]CIRM - Université de Lausanne, Sion, Switzerland
[11]Int. ecorisQ Association, P.O. Box 2348, 1211 Geneva 2, Switzerland

Correspondence: Dorren, Luuk (luuk.dorren@bfh.ch)

Abstract. At present, a quantitative basis for delimiting realistic rockfall runout zones on the basis of trajectory simulation data is generally missing. The objective of this study is to come up with standardized reach probability threshold values ($RPTV$) to separate "realistic" from "unrealistic" simulated rockfall runouts. We therefore compared reach probability values ($Preach$) simulated with Rockyfor3D for 458 mapped, fresh rockfall blocks (silent witnesses SW) on 18 different sites with a volume >= 0.05 m^3 and estimated occurrence frequencies up to 300 years. We analysed which block, slope and forest characteristics influenced $Preach$ of the SW based on a linear mixed effects model. The results indicate that the limit of a realistic runout zone lies in the range where simulated $Preach$ values are between >1% and approximately 3%. We conclude that $RPTV$ can be defined to values lying in the range from 1.2% to 2.5% depending on the defined block volume and the encountered cumulative basal area in a forested transit zone. Where possible, the defined $RPTV$ should be compared and validated by field recordings of SW.

keywords: rockfall hazard modelling; simulation, Rockyfor3D, silent witness, statistical analysis

1 Introduction

Throughout the world, at places where steep rocky slopes occur, the sudden and rapid downslope movement of single rock fragments, blocks or fragmented rock masses threatens human life and poses problems for infrastructure and residential areas. For example, such processes, popularly referred to as rockfall, are expected to cause an estimated yearly damage of 12 million

Natural Hazards and Earth System Sciences
Discussions

CHF to the Swiss national road network (Arnold and Dorren, 2015). Cliffs that are known to pose imminent rockfall threats to the underlying damage potential can be monitored using extensometers and/or remote sensing such as radar interferometry, laser scanning or photogrammetry (see Abellán et al., 2010; Derron and Jaboyedoff, 2010; Caduff et al., 2015; Farmakis et al., 2020; Guerin et al., 2020). On locations where the threat is less imminent, risk reduction is generally achieved through spatial planning, technical measures, such as rockfall dams (Lambert et al., 2013; Kanno et al., 2020) and flexible nets (Caviezel et al., 2020; Lambert et al., 2020; Tahmasbi et al., 2020), and biological measures (i.e., protection forests; Dorren et al., 2005a; Moos et al., 2017; Lanfranconi et al., 2020; Scheidl et al., 2020).

An important basis for the implementation of above-mentioned types of measures is the rockfall hazard and risk assessment. Although such assessments have been improved considerably over the last decades, it remains a challenge to fully grasp the unknowns of rockfall processes with respect to space and time (Crosta et al., 2015). These are related to a range of factors which include: precise release locations in a rock cliff (cf. Loye et al., 2009), the frequency and initial volume of the released rock mass (cf. Francioni et al., 2020; Farvacque et al., 2021; Hantz et al., 2021), the fragmentation, i.e. disaggregation of the initial volume during the failure process and breakage after the first and subsequent impacts (cf. Giacomini et al., 2009; Ruiz-Carulla et al., 2015; Matas et al., 2020; Ruiz-Carulla and Corominas, 2020), the size and shape and change thereof of the individual rockfall fragments that propagate down the slope (c.f., Melzner et al., 2020), the transformation and dissipation of energy during rebounds on the slope surface (Caviezel et al., 2021) and impacts on standing or lying tree stems (Dorren and Berger, 2006; Dorren et al., 2006; Lundström et al., 2009; Lu et al., 2020; Noël et al., 2021; Ringenbach et al., 2021), penetration depth in the soil and alteration of the terrain during impact (Pichler et al., 2005; Wang and Cavers, 2008; Guangcheng et al., 2015; Lu et al., 2019). To come up with realistic predictions of the areas that are potentially endangered by rockfall processes, modelling rockfall trajectories is one of the methods that provide an important information (Volkwein et al., 2011; Yan et al., 2020). To account for some of the above mentioned uncertainties and to the intrinsic variability of rockfall as function of block shape, volume, exact initial position, etc., trajectory simulation models generally use stochastic variables in their algorithms (e.g., Bourrier et al., 2009). Since such probabilistic computational algorithms rely on repeated random sampling, also referred to as a Monte Carlo method (Von Neumann and Ulam, 1951), the numerical results are presented as probability distributions (Farvacque et al., 2020). In case of rockfall trajectory simulations, these generally include data on runout zones, kinetic energies, and passing heights for all simulated individual rockfall blocks sometimes converted into individual risk estimates (Farvacque et al., 2019a).

Although attempts have been made to automatize the delineation of hazard zones on the basis of trajectory modelling (e.g., Jaboyedoff et al., 2005; Abbruzzese et al., 2009; Abbruzzese and Labiouse, 2020; Farvacque et al., 2020), in the daily practice this delineation is mostly based on human interpretation of the simulation results and subsequent definition of the realistic runout zone for a given simulated scenario. Thereby, extreme long, low probability trajectories are separated from all other trajectories in the modelled rockfall runout distribution based on expert judgement, eventually supported by historical records, mapped deposited rocks (silent witnesses SW), and other information recorded in the field (e.g., tree impacts). Legal considerations varying from one country to another also play a role, with often no clear correspondence between sound statistical and probabilistic concepts (Eckert et al., 2018). The basis provided by rockfall trajectory models for doing so is data on the number of passages per cell normalised by the total number of blocks potentially passing through a cell, which depends on the number of simulations per source cell and the number of feeding source cells. This normalised model output data can be referred to as reach probability data. The reach probability is a conditional probability depending on whether a block is released or not. At present, no standardized reach probability threshold values ($RPTV$) are defined for delimiting rockfall runout zones based on trajectory simulation data. This is usually done in a very subjective manner. Therefore, expert knowledge still represents a great deal in rockfall hazard assessment.

A sound statistical comparison of simulation-based reach probability values with field mapped stopping locations of blocks from recent rockfall events could improve the quantitative basis for the delimiting rockfall runout zones. Consequently, the objective of this study is to come up with a quantitative basis for defining $RPTV$ by comparing reach probabilities simulated with a three-dimensional rockfall model for mapped, fresh SW of 18 sites in Austria, France, Greece, Italy and Switzerland for which the runout distance return period could be estimated as being maximum 300 years. In this paper we analyse which reach probability values are typically expected in the outer range of the rockfall runout zones and quantify which block, slope and forest characteristics influence the simulated reach probabilities of the mapped SW.

2 Materials and Methods

2.1 Study sites and mapping of SW

For this study, we used data from 18 different rockfall sites in Europe (Fig. 1) with a total of 769 mapped SW (see table 1). To analyse the effect of the complexity of the topography at the study site, we classified each study site in topography type 1 (simple topography: linear cliff with an underlying linear transit - mainly talus - slope), 2 (intermediate complex topography) and 3 (complex topography: gullys and superposed cliffs, large variability in slope gradients) according to the examples in Fig 2. The mapped SW correspond to stopping locations of blocks mapped in the field. Only fresh blocks were taken into account, meaning that blocks with weathered surfaces as well as those partly buried by material covering the surrounding slope surface were not recorded (Fig. 3). Preferable, we also detected additional rockfall marks such tree wounds and rockfall impact signs (craters) upslope from the mapped SW. The block volume (Vol) of each SW was calculated on the basis of the measured width, depth and height, as well as an estimated rounding factor varying from 0.52 (a perfect sphere) to 1 (a perfect rectangle). All data on the SW was gathered by the authors, except for the Gurtnellen site in Switzerland (CH), which was provided by (Thali, 2009). At every site, we focused at mapping SW which, based on an expert interpretation (i.e., comparison with deposits in the direct surroundings, block volumes recorded in historical events databases of the region) corresponded to blocks that resulted from recent rockfall events with return periods of max. 300 years in terms of runout distance. Similarly, very frequent events were excluded from the analysis (cf., 2.3), so as to work with a sample of rockfall runout events that may well separate safe from unsafe locations in terms of hazard mapping for buildings and infrastructure.

Generally, we can distinguish 4 main types of mapped SW for the study sites (cf. table 1). At the Taesch (CH) study site, all deposited blocks of the rockfall event of August 2013 were mapped. At the Claro (CH), Flaesch (CH), Orvin (CH, c.f., Moos et al., 2018), Schmitten (CH) and Tithorea in Greece (GR) (, c.f., Saroglou et al., 2015) study sites, we mapped all de-

https://doi.org/10.5194/nhess-2022-32
Preprint. Discussion started: 4 February 2022

Natural Hazards and Earth System Sciences
Open Access
Discussions

posited rockfall blocks of multiple recent rockfall events. At six other study sites, we mapped selected freshly deposited blocks which had either a large Vol in comparison to surrounding blocks or a longer runout distance compared to the majority of the deposited blocks, meaning that they are deposited in the lower range of the propagation zone) of one specific recent rockfall event (Gurtnellen (CH), event of May 2006; Varces in France (FR), event of December 2008; Veyrier (FR), event of January 2009; Tramin in Italy (IT), event of January 2014; Evolène (CH), event of October 2015; Vaujany (FR), rockfall experiments of October 2003 (c.f., Dorren et al., 2005b). Finally, at another six sites, we mapped selected blocks present at the study site which resulting from multiple rockfall events (e.g., Crolles in FR; cf., Farvacque et al., 2019b). We also mapped and recorded field data required for the modelling (terrain roughness as well as soil types), following an intensive exchange on a common field mapping/recording method, corresponding to the Rockyfor3D manual (Dorren, 2016).

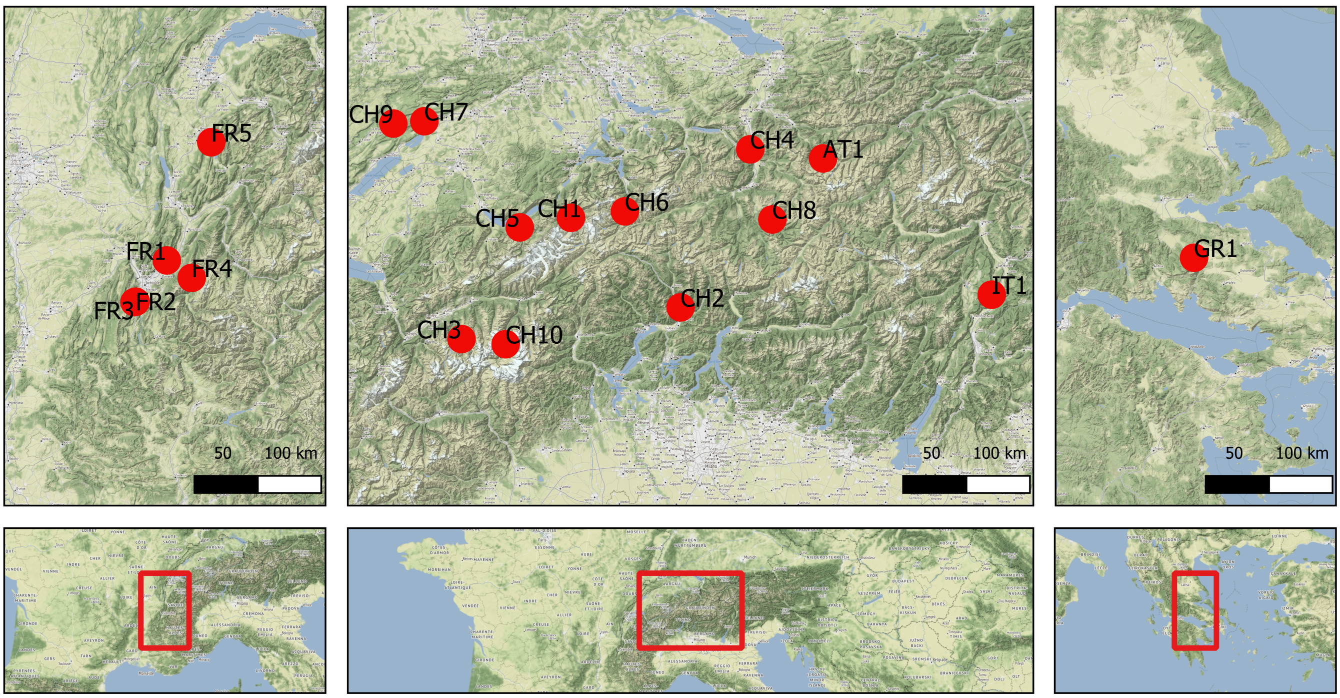

Figure 1. Upper row: maps showing the location of all study sites. Bottom row: overview maps showing the coverage of the maps above, centered on the French Alps, Switzerland and Greece - from left to right. Background: Stamen Terrain (under CC BY 3.0).

https://doi.org/10.5194/nhess-2022-32
Preprint. Discussion started: 4 February 2022

Natural Hazards and Earth System Sciences
Discussions

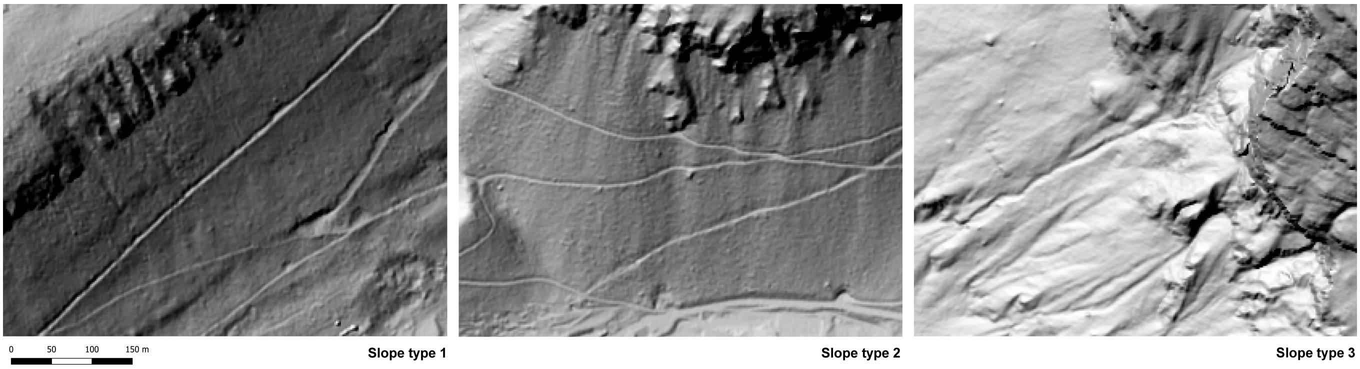

Figure 2. Visualisation of the three topography types used in this study. Type 1: simple topography (linear cliff with an underlying linear transit - mainly talus - slope); type 2: intermediate complex topography; type 3: complex topography (gullys and superposed cliffs, large variability in slope gradients)

To characterise the forests at the study sites, we used an approach combining 1) mapping of forest stands based on orthophotos or, if available, high-resolution vegetation height models derived from airborne laser scanning data or drone flights and 2) forest inventory plots in the field. At least one representative plot of 10 by 10 m or 20 x 20 m (depending on the tree density) was inventoried for each homogeneous forest stand type in the different study areas. From those inventory plots, we derived the required forest data for the used rockfall trajectory simulation model (cf. section 2.2).

Figure 3. Left: the block of 6.25 m3 which fell in 2009 in Veyrier-du-lac (FR) is an example of a SW taken into account in this study (Photo: F.Berger). Right: the ancient block of approx. 150 m^3 lying upslope from the village Veyrier-du-lac, with a tree growing on top of it, has been left out from our analysis because the event had an estimated return period tat is larger than 300 years (Photo: ONF-RTM).

https://doi.org/10.5194/nhess-2022-32
Preprint. Discussion started: 4 February 2022

Natural Hazards and Earth System Sciences
Open Access
EGU
Discussions

2.2 Monte-Carlo based rockfall trajectory simulation model

The Monte-Carlo based rockfall simulation model used in this study is Rockyfor3D (for details see (Dorren, 2016)), which is a probabilistic, process-based rockfall model simulating trajectories of individual blocks in three dimensions. Rockyfor3D was developed on the basis of full-scale rockfall experiments in the field and uses raster maps describing topography (Digital Elevation Model - DEM), rockfall source cells, the mechanical properties of the surface material and the slope surface roughness. To represent the forest, the model requires the number of trees, the mean and standard deviation of stem diameters at breast height (DBH), as well as tree types (coniferous or broadleaved) per cell as input data (Dorren et al., 2004, 2006). For each rockfall source cell, the trajectories of a given number of rocks are simulated by considering flying and bouncing (rebounds on the surface). The density as well as the indentation resistance (cf. (Pichler et al., 2005), which have an effect on the penetration depth of the block during a impact before rebounding (which in turn affects the tangential energy loss of the block) and dampening effect (represented by the normal coefficient of restitution Rn) of the impacted material is defined by the following eight soil types:

- $Soiltype$ 0 = River, or swamp, or material in which a rock could penetrate completely (Rn = 0)
- $Soiltype$ 1 = Fine soil material (depth > 100 cm; Rn = 0.21 - 0.25)
- $Soiltype$ 2 = Fine soil material (depth < 100 cm), or sand/gravel mix in the valley (Rn = 0.30 - 0.36)
- $Soiltype$ 3 = Scree (material fragments Ø < 10 cm), or medium compact soil with small rock fragments, or forest road (Rn = 0.34 - 0.42)
- $Soiltype$ 4 = Talus slope (material fragments Ø > 10 cm), or compact soil with large rock fragments (Rn = 0.39 - 0.47)
- $Soiltype$ 5 = Bedrock with thin weathered material or soil cover (Rn = 0.21 - 0.25)
- $Soiltype$ 6 = Bedrock (Rn = 0.48 - 0.58)
- $Soiltype$ 7 = Asphalt road (Rn = 0.32 – 0.39)

Surface roughness is represented by three raster maps. These rasters represent deposited rocks and rock fragments covering the slope surface, which form "obstacles" for the falling block. Micro topography (e.g., steps in the terrain) should not be taken into account here. The surface roughness was recorded in the field by identifying homogeneous zones in the study areas. These were represented as polygons on a map (in most cases printed hillshade maps) and later digitised and rasterised. Each polygon defines the surface roughness, expressed in the size of the material covering the slope's surface, looking in the downward direction of the slope. Three roughness probability classes need to be represented by a raster map and correspond to the height of a representative obstacle in m that a falling block encounters in resp. 70%, 20%, and 10% of the cases during a rebound in the defined polygon. If the slope surface is smooth, a roughness value of 0 m was used. The choice of the roughness values needs careful attention, since Rockyfor3D is sensitive to this parameter.

During each simulated rebound on slopes with a gradient less than 30°, Rockyfor3D decreases the slope angle at the position of the rebound at random (following a uniform distribution), similar to (Pfeiffer and Bowen, 1989), up to a maximum decrease of 4°. Rolling is represented by a sequence of short-distance rebounds with a distance in between that is equal to the radius of the block and an absolute minimum distance of 0.2 m. Rockyfor3D explicitly calculates the deviation and energy loss after impacts with trees dependent on the DBH, impact position, and the kinetic energy of the rock before the impact.

The main output of RockyFor3D used for this study consists of a raster map containing information on the reach probability (cf. section 2.3. Additional outputs generated by Rockyfor3D are, amongst others, raster maps with information on the kinetic energies, the passing heights, the number of deposited rocks, the number of tree impacts per cell and the angle of the straight line between source and stopping cell (energy line angle ELA; see Dorren, 2016).

We simulated the exact Vol mapped for each site with Rockyfor3D using a rectangular block shape and extracted the simulated reach probabilities for the position of the deposited blocks. We simulated 100 blocks per start cell. At all sites, we used elevation models with a resolution of 2 x 2 m, except for the Greece study site, where only a 5 x 5 m resolution DEM was available.

2.3 Reach probability

The reach probability ($Preach$) value in a given cell x indicates the probability (given in%) that cell x is reached by a block that has detached from the cliff. It is calculated by:

$$Preach_{(x)} = \frac{NB_{(\mathrm{x})} \cdot 100\%}{Nsims \cdot Nsources_{(x)}} \tag{1}$$

Where $NB_{(x)}$ is the number of blocks passed through cell x, $Nsims$ is the number of individual blocks simulated from each source cell and $Nsources_{(x)}$ is the number of source cells "feeding" cell x. In other words, the reach probability is a measure of the number of simulated blocks passed through a given cell relative to the number of blocks potentially "feeding" the cell. It is typically used as indicator to determine the rockfall runout zone of a given release area. However, a quantitative basis for differentiating the realistic $Preach$ values from the extreme ones (in terms of runout distance) which can therefore be neglected for hazard mapping, is missing. In this study, we extracted for each SW the simulated $Preach$ as the mean of the $Preach$ values > 0 in the eight neighboring cells as well as in the center of a mapped SW. This value is hereafter referred to as $Preach_{SW}$. We excluded SW with a Vol < 0.05 m^3 and a $Preach_{SW}$ > 5% from the originally 769 SW, since they were regarded as irrelevant for hazard analysis or are not in the outer reach, respectively. The threshold of 5% was determined based on a two-step outlier detection according to (Yang et al., 2019) using the median absolute deviation as score. In total, 202 SW from 9 sites were not reached by any simulated trajectory, i.e. their deposit location could not be reproduced by the rockfall simulation. All these SW had a significantly smaller Vol than the neighbouring SW which were perfectly reached by the simulations (Fig. 4). We therefore assumed that these SW are most likely fragments of larger blocks that broke off while falling down slope. On the basis of this assumption, we excluded those SW from the analysis. This resulted in 458 SW with a Vol > 0.05 m^3 and with a $Preach_{SW}$ > 0 and <= 5%.

https://doi.org/10.5194/nhess-2022-32
Preprint. Discussion started: 4 February 2022

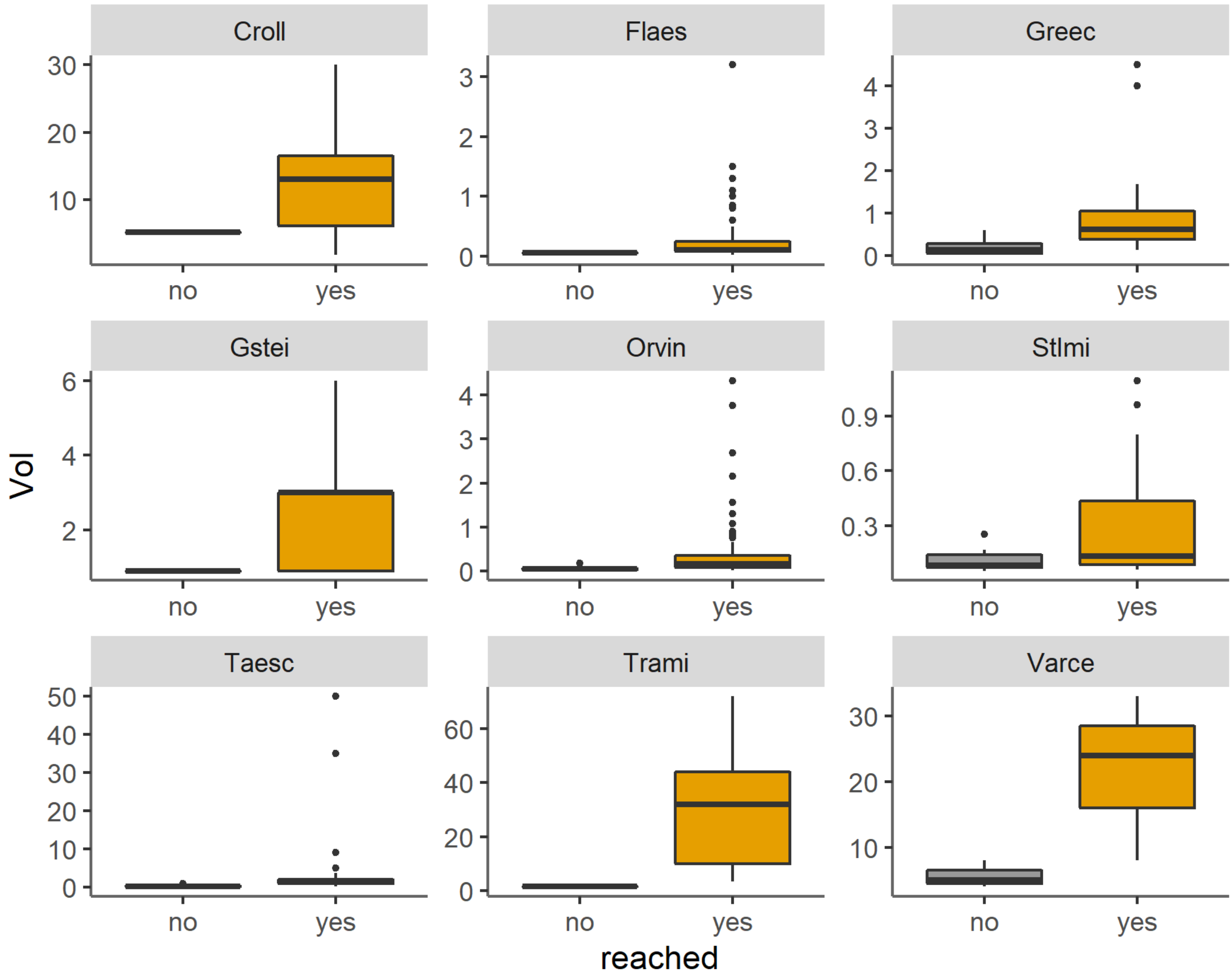

Figure 4. Distribution of block volumes (Vol; y axis) depending on whether they were reached or not (yes / no) by a simulated rockfall trajectory. Only the sites where not all SW were reached are presented.

2.4 Statistical analyses of the simulation results

We analysed which block, slope and forest characteristics influenced $Preach_{SW}$ of the SW that were reached by the simulations (n=458). We first tested whether there are significant differences in $Preach_{SW}$ between sites as well as between Vol classes based on a one-way Anova with a logarithmic transformation of $Preach_{SW}$ using the *aov* function of the *stats* package
165 in the statistical software R. We then fitted a linear mixed effects model (lmm) for $Preach_{SW}$ with the variables reported in table 2 as fixed effects and the site as random effect. Here, cbA is the normalised cumulative basal area along a given trajectory, which is calculated by the mean basal area of forested area [$m^2.ha^{-1}$] x trajectory length [m] / 100 m. The lmm (*fit.lmm*)

Natural Hazards and Earth System Sciences
Open Access
EGU
Discussions

was fitted to the log-transformed $Preach_{SW}$ values with stepwise backward variable selection with the aim to minimize the Akaike Information Criterion (AIC) using the *step* function (*lmerTest* package; (Kuznetsova et al., 2017)). We only included explanatory variables that were not substantially correlated (Spearman correlation coefficient < 0.4) to avoid colinearity. We also tested for possible variable interactions, which did not substantially improve the model. The lmm was implemented with the *lmer* function of the *lme4* package in the statistical software R (Bates et al., 2015). P-values were obtained by *Wald-Chisq* tests as well as likelihood ratio tests of the full model against the model without the variable in question. The model performance was assessed based on customary residual plots (Stahel, 2017) and the marginal and conditional R^2 (Nakagawa and Schielzeth, 2013). We further fitted a random forest model (rfm) (Breiman et al., 1984) and compared predicted values of the lmm to the predicted values from the rfm. The latter was implemented using conditional inference trees as base learners in the *cforest* function of the party package in the software R (Strobl et al., 2009; Hothorn et al., 2010). The random forest model was fitted using three times repeated 10-fold cross-validation to reduce the risk of overfitting (Kohavi et al., 1995)).

Table 2. Explanatory variables used in the linear mixed effects model (lmm) and the random forest model (rfm) predicting the $Preach$ of the SW.

Variable	Description	Data type
$Slope_{mean}$	Mean slope of a block trajectory between the deposition of the block and release area (rock cliff) [°]	numerical
$cliffHeight$	Vertical difference between the top and bottom of the rock cliff (height of the release area) [m]	numerical
$VolClass$	Rock volume class [m^3] (1=<0.05; 2=0.05-0.2m; 3=0.2-0.5; 4=0.5-1; 5=1-2; 6=2-5; 7=5-10; 8=10-20; 9=20-50; 10=50-100; 11=100-200; 12=$\geq$200)	categorical
$SlopeType$	Categorization of slope type (1 = simple topography; 2 = intermediate complex topography; 3 = complex topography)	categorical
$Rg70_{maj}$	Majority of roughness values of 70 % of the surface along trajectory [m]	numerical
$Soiltype_{maj}$	Majority of soiltype values along trajectory (type 1 to 5 with decreasing dampening capacity of soil)	categorical
cbA	Normalised cumulative basal area along trajectory [$m^2.ha_{-1}$]	numerical

3 Results

The mean $Preach_{SW}$ of the considered 458 SW was 1.79% and the median $Preach_{SW}$ was 1.41% (Fig. 5). 75% of the 458 SW had a $Preach_{SW}$ <= 2.02%. This corresponds to, on average, 1247 simulated trajectories that attained the mapped SW (min = 36; max = 14526).

https://doi.org/10.5194/nhess-2022-32
Preprint. Discussion started: 4 February 2022

Natural Hazards and Earth System Sciences
Discussions

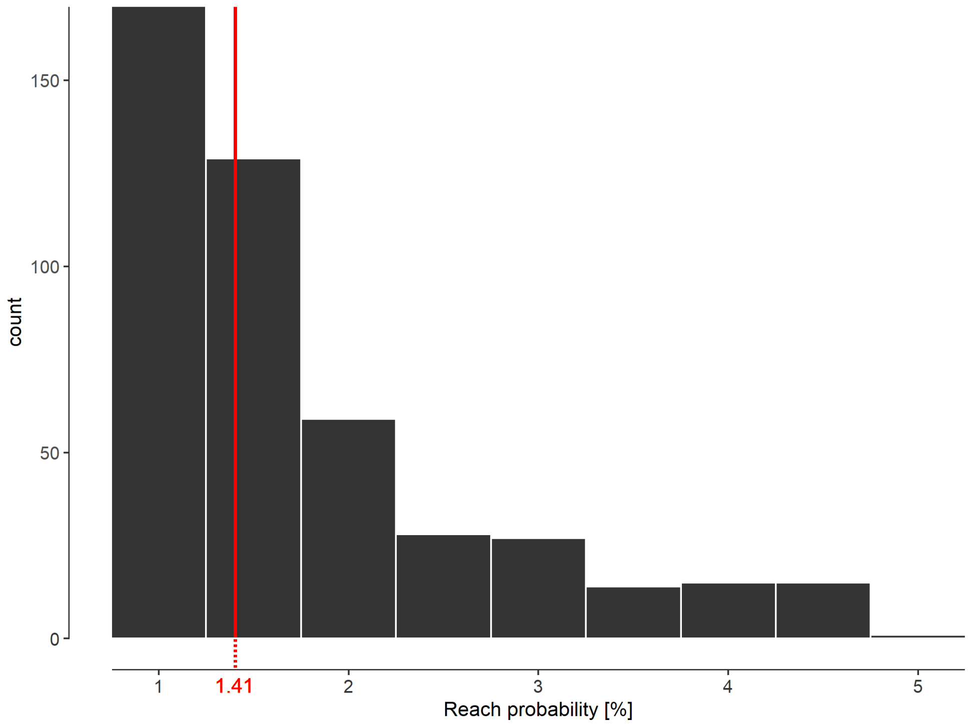

Figure 5. Histogram of reach probabilities $Preach_{SW}$ of SW with Vol >= 0.05 m^3 and $Preach_{SW}$ >0% and <=5% at all sites with the median value of 1.41 %.

The Anova revealed a significant difference between sites, whereby the Tukey post-hoc test showed that only Claro and Taesch significantly differ from the others (Fig. 6), meaning that only the SW of these two sites have significantly different $Preach$ values. Furthermore, the analyses showed that $Preach_{SW}$ is significantly higher for blocks with a Vol of 5-10 m^3 (Fig. 7).

https://doi.org/10.5194/nhess-2022-32
Preprint. Discussion started: 4 February 2022

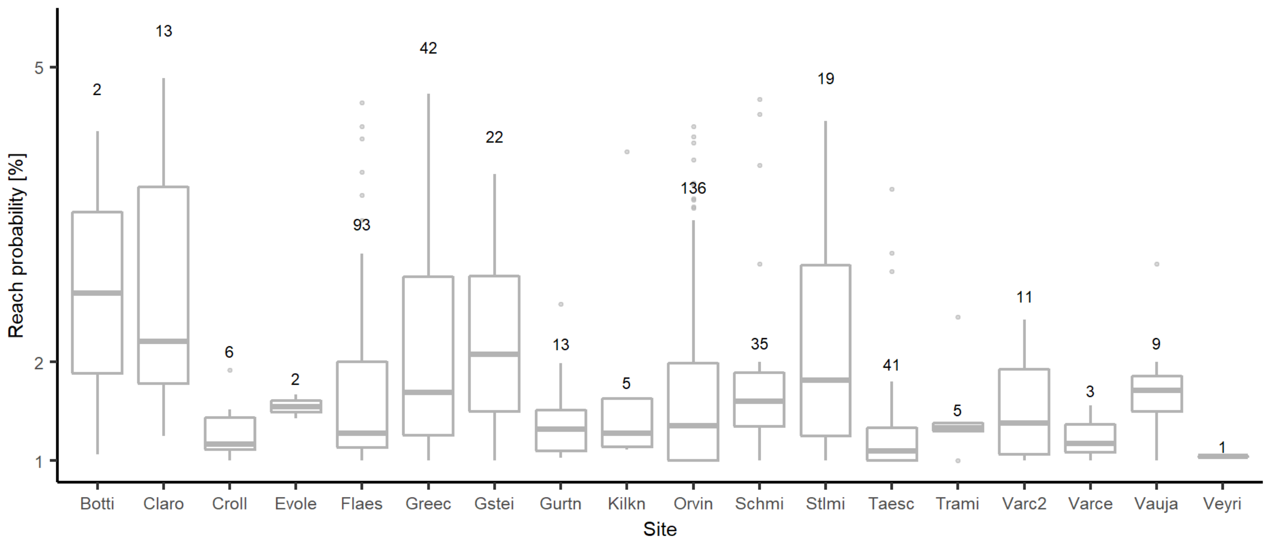

Figure 6. Box plot of simulated reach probability values [in %] at the different sites for SW with Vol >= 0.05 m^3 and $Preach_{SW}$ >0% and <=5%. n = number of measured SW at each site.

According to both the lmm and the rfm, $Preach_{SW}$ is significantly influenced by the block volume class ($VolClass$), the normalized cumulative basal area (cbA), the mean slope ($Slope_{mean}$) and the soil roughness ($rg70_{maj}$; cf. Table 3). The different soil types ($soiltype_{maj}$) were not significant in the lmm, but remained in the final model. $Preach_{SW}$ for a given
190 SW increases with increasing Vol, whereas it decreases again for the largest $VolClass$ (Figure 7), for increasing cumulative basal area of the forest (Figure 8), increasing slope angle, decreasing soil roughness and decreasing dampening capacity of the soil. The lmm explains 45% of the variance (conditional R^2). There is a relatively high correspondence between the predicted values of the lmm and the rfm with slightly smaller values predicted by the lmm model (Fig. 9).

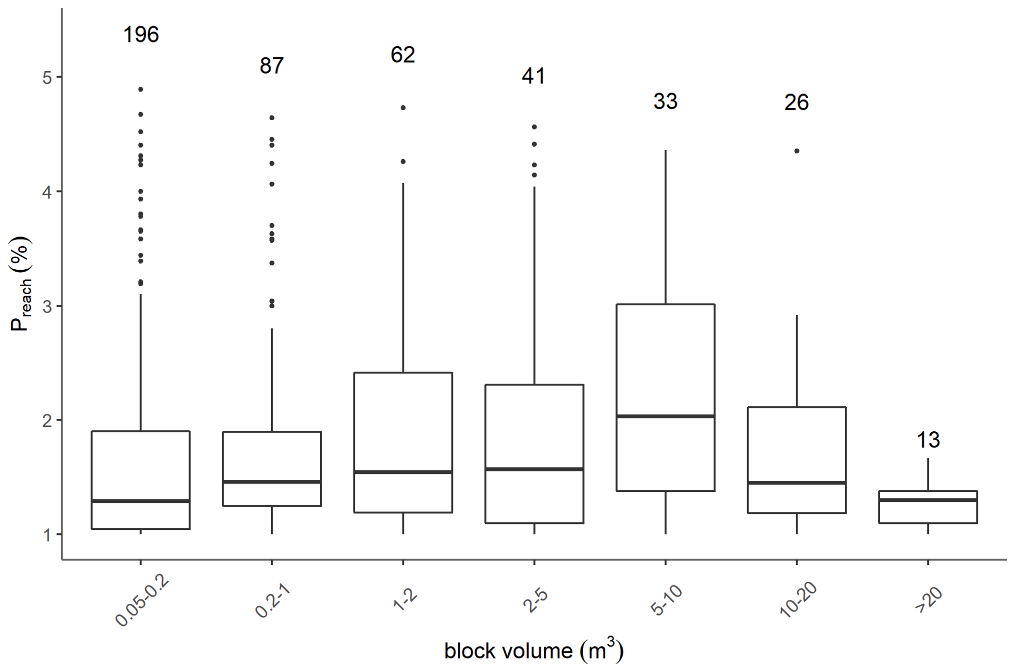

Figure 7. Box plot of reach probability values per volume class ($VolClass$). The number of observations is given above the box plots.

https://doi.org/10.5194/nhess-2022-32
Preprint. Discussion started: 4 February 2022

Natural Hazards and Earth System Sciences
Open Access
Discussions

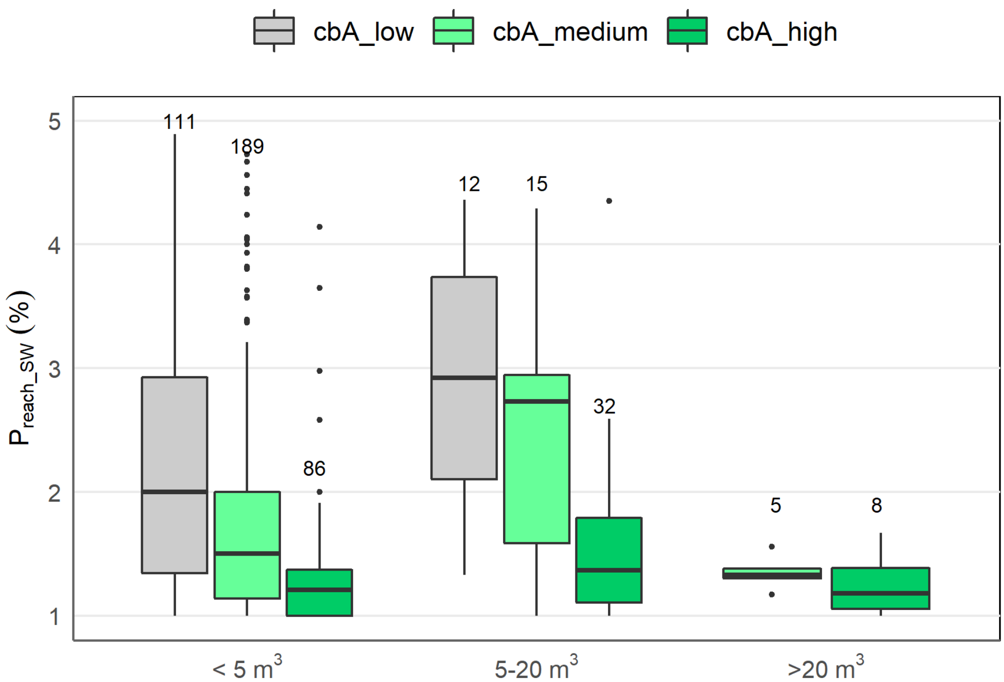

Figure 8. Box plot of $Preach_{SW}$ values as function of the normalized cumulative basal area (cbA) and the block volume (Vol), whereby three classes of cbA (cbA_{low}: cbA <= 20 $m^2.ha_{-1}$; cbA_{medium}: cbA = 20-80 $m^2.ha_{-1}$; cbA_{high}: cbA > 80 [$m^2.ha_{-1}$]) and three block block volume classes ($VolClass$) (Vol. < 5 m^3; Vol. = 5-20 m^3; Vol. > 20 m^3) were distinguished. The number of observations is given above the box plots.

https://doi.org/10.5194/nhess-2022-32
Preprint. Discussion started: 4 February 2022

Table 3. Variance and standard deviation of random effect (upper table) and estimates with standard errors, and p values of the coefficients of the fixed effects (lower table) of the linear mixed effects model for $Preach_{SW}$

Random effect	Variance	Std. Dev.	
Site	0.02	0.15	
Residual	0.12	0.34	
Fixed effects	Estimate	Std. Error	p value
Intercept	0.54	0.44	0.22
Vol. 0.2-1 m^3	0.13	0.05	0.003
Vol. 1-2 m^3	0.19	0.06	0.0007
Vol. 2-5 m^3	0.40	0.07	$1.5*10^{-8}$
Vol. 5-10 m^3	0.42	0.10	$5.3*10^{-8}$
Vol. 10-20 m^3	0.52	0.12	$3.9*10^{-7}$
Vol. > 20 m^3	0.16	0.14	0.03
$rg70_{maj}$ (log)	-0.1	0.03	0.0003
$soiltype_{maj}$ 1	-0.13	0.51	0.80
$soiltype_{maj}$ 3	-0.29	0.37	0.44
$soiltype_{maj}$ 4	-0.22	0.38	0.55
$soiltype_{maj}$ 5	0.06	0.38	0.88
cbA (log)	-0.20	0.02	$< 10^{-16}$
$Slope_{mean}$	0.01	0.003	0.0002

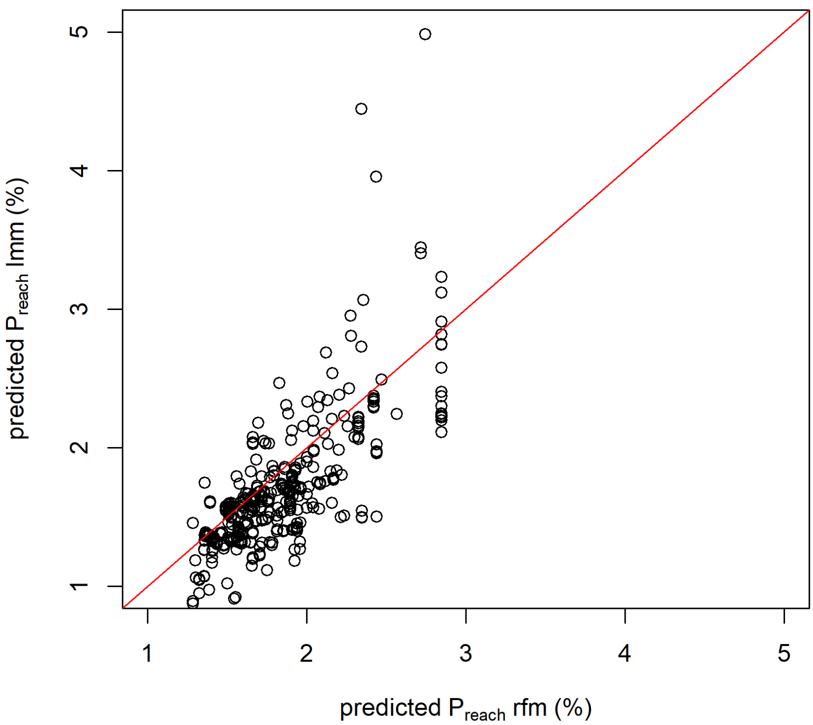

Figure 9. Reach probability values predicted by the mixed linear model (lmm; y-axis) vs. values predicted by the random forest model (rfm; x-axis).

4 Discussion

The results of our analysis of a large number of deposited blocks from 18 sites in Europe imply that the lower limit of rockfall runout zones typically have $Preach$ values, simulated with RockyFor3D, between 1 and 3%. The statistical models showed that the $Preach$ values, simulated with Rockyfor3D, of deposited blocks strongly depend on block, slope and forest characteristics. Smaller $Preach$ values are in particular achieved for blocks with a volume between 5 and 10 m^3 and densely wooded forest (cbA > 20 m^3). The analysis provides important information for the interpretation of simulation results for rockfall hazard mapping.

This study is conceptually based on the assumptions that the SW analyzed in this study were all registered in the typical outer range of a rockfall propagation zone, as it is typically done for hazard and risk assessment. However, we used a collection of study sites where different field protocols, especially with regards to the used criteria for SW recording, were applied. There are sites where only blocks with an "extreme" runout were recorded (e.g. Evolène) and others, where deposits also in the upper part of the slope were recorded (e.g. Orvin). There might thus be a slight bias regarding the range of $Preach$ values used in this study. We attempted to offset this by excluding all SW with a $Preach$ > 5%.As already mentioned, an important bias is very probably the result of the recording of SW corresponding to block fragments (cf. fig. 4). Fragmentation is extremely common during rockfall processes and leads to difficulties when deciding on representative block shape and block size in the hazard analysis process (Jaboyedoff et al., 2005; Matas et al., 2020). In the field, it is rarely possible to differentiate which deposited blocks resulted from fragmentation in the rock cliff, or upon first impact below the cliff, or in the lower parts of the transit area. This has been one of the arguments to keep all mapped SW in the original data set. It allowed us to profit from the large data source on different sites and slope conditions. The analysis of the volume distribution of SW that were not reached by the simulations finally clearly indicated that these SW were block fragments and, thus, we excluded them in the final data set.

The developed statistical model shows that $Preach$ values increase with increasing Vol, increasing slope angle,decreasing forest cover, and decreasing soil roughness. These factors promote an acceleration of the falling blocks leading to longer runout distances. Thus, we can conclude that on slopes with favorable characteristics for rockfall propagation, the probability that rocks in reality end up in the extreme range of the propagation zone increases. The fitted regression model yields an R^2 of 48% and the residual analysis, too, indicating that the model fits the data relatively well. The predicted $Preach$ values of the regression model and the random forest model correspond well, suggesting that the two models are relatively robust.

The results indicate that the limit of a realistic runout zone lies in the range where simulated $Preach$ values are between >1% and approx. 3% (= 70%-ile of all considered SW). As a basic rule, based on the median and mean $Preach$ values presented here as well as on long-term practical experience, we would recommend choosing a $RPTV$ larger than 1% and smaller than 2% in a first step. If abundant data on field mapped SW allows for a detailed comparison with the simulated data, the $RPTV$ can be eventually increased when supported by the field observations. Here, one must be sure, that blocks with extreme runout distances were not removed in the field, as is often done by farmers (in agricultural fields) or by infrastructure managers (on road and railways). To eventually come with actual probabilities of a block having "extreme" runout, propagation probabilities have to be combined with the release frequencies of expert defined homogeneous release areas in a rock face.

When interpreting simulated $Preach$ values, it is important to execute a sufficiently large number of simulations per start cell, to make sure that the $Preach$ in the lower ranges of the runout zone converge. To do so, experience shows that at least 100 simulations per start cell are required. An analysis in the study site St. Paul de Varces (FR) showed that there is, however, no significant difference, even in the raster cells with low $Preach$ values, between 100 or 1000 simulations per source cell. For some areas, due to a topographic configuration leading to strongly diverging trajectories, it might be necessary to simulate 200 or in extreme cases 500 trajectories per start cell. Though for most model simulation based rockfall hazard analyses in the practice, 100 simulations per start cell will be sufficient. Furthermore, $Preach$ depends on the definition of the source area and can possibly be affected by the size, form and position of the source area. A known problem occurs when two or more source areas are superposed on a slope with a transit area between them. If some blocks from the upper source area fall over the rock face below this locally results in a higher number of sources underneath the rock face below, whereas the number of passages

https://doi.org/10.5194/nhess-2022-32
Preprint. Discussion started: 4 February 2022

does not increase significantly. Finally this leads to lower $Preach$ values compared to neighbouring cells which were only fed by the lower rock face. In such a case, it might be useful to simulate each of the superposed source areas separately.

To come up with more detailed categories of $RPTV$, we applied the developed lmm model to predict $Preach$ values for diverse Vol as well as varying slope and forest characteristics. The derived $RPTV$ categories are presented in Fig 10. As shown by table 3, the key data required for defining $RPTV$ is finally the Vol and the cbA. For the latter, one can roughly differentiate between low, medium and high cbA. Low cbA represents a basal area (G) of 20 to 30 m^2/ha with a trajectory length up to 50 m (measured along the slope). Medium cbA represents a G of 20 to 30 m^2/ha with a trajectory length of 50 to 250 m or a G of 50 m^2/ha with a trajectory of 50 to 100 m. A high cbA represents a G of 20 to 30 m^2/ha with trajectory lengths > 250 m or a G of 50 m^2/ha with trajectories longer than 150 m.

Finally, we do not recommend to delineate limits of rockfall hazard zones only based on rockfall simulations without the expert interpretations and the comparison and validation with field observations. To increase the quantitative basis on simulated $Preach$ values, further analyses on additional data sets, based on a standardized field recording protocol, are recommended.

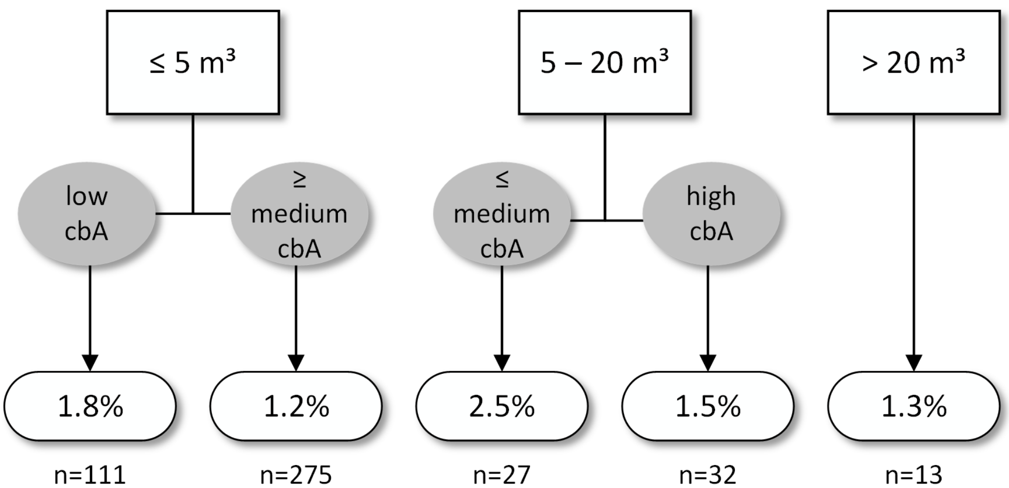

Figure 10. Summary of the results of the lmm model serving as a basis for defining the $RPTV$ to be used in the practice based on the Vol and the cbA. The reported $Preach$ values correspond to the median of the respective classes. The number of observations is indicated by n.

5 Conclusions

On the basis of the presented results, we conclude that simulated $Preach$ data are a valuable basis for delimiting a rockfall runout zone downslope from a release area. The limit of a realistic rockfall runout zone for rectangular rocks simulated with Rockyfor3D lies in the range where $Preach$ values are between >1% and, depending on the Vol, slope roughness and the type and area of forest cover, smaller than 3%. As a basic rule, we therefore recommend choosing a $RPTV$ larger than 1% and depending on the before mentioned variables, $RPTV$ can be defined in detail and fixed to values lying in the range from 1.2% to 2.5%. We recommend to delimit runout zones based on rockfall simulations only in combination with expert-based site interpretations and, if possible, validation with historical events on the basis of increasingly available extensive inventories (Rupp and Damm, 2020; Eckert et al., 2020). Cross-validation of the results with other modelling approaches are also strongly advised. To improve the quantitative basis presented in this article, analyses of additional similar data are desirable.

Author contributions. Conceptualization, L.D., C.M.; Methodology, L.D., N.E., F.Bo., C.M.; Field data, L.D., F.Be, H.S., D.T., H-H.U., C.M.; Simulations, L.D.; writing—original draft preparation, L.D., C.M.; writing—review and editing, L.D., F.Bo, M.Sc., M.St., H-H.U., C.M., N.E.; visualization, L.D., C.M.; All authors have read and agreed to the published version of the manuscript.

Competing interests. No competing interests are present

Acknowledgements. We would like to acknowledge Daniel Büttner, Jacqueline Ernst, Bernhard Maier, Eric Mermin, Pascal Tardif and David Toe for assisting in field data collection. INRAE is member of Labex OSUG.

https://doi.org/10.5194/nhess-2022-32
Preprint. Discussion started: 4 February 2022

References

Abbruzzese, J. M. and Labiouse, V.: New Cadanav Methodology for Rock Fall Hazard Zoning Based on 3D Trajectory Modelling, Geosciences, 10, https://doi.org/10.3390/geosciences10110434, 2020.

Abbruzzese, J. M., Sauthier, C., and Labiouse, V.: Considerations on Swiss methodologies for rock fall hazard mapping based on trajectory modelling, Natural Hazards and Earth System Sciences, 9, 1095–1109, https://doi.org/10.5194/nhess-9-1095-2009, 2009.

Abellán, A., Calvet, J., Vilaplana, J. M., and Blanchard, J.: Detection and spatial prediction of rockfalls by means of terrestrial laser scanner monitoring, Geomorphology, 119, 162–171, 2010.

Arnold, P. and Dorren, L.: The importance of rockfall and landslide risks on Swiss national roads, in: Engineering Geology for Society and Territory - Volume 6, edited by Lollino, G., Giordan, D., Thuro, K., Carranza-Torres, C., Wu, F., Marinos, P., and Delgado, C., pp. 671–675, Springer International Publishing, Cham, 2015.

Bates, D., Mächler, M., Bolker, B., and Walker, S.: Fitting linear mixed-effects models using lme4, Journal of Statistical Software, 67, https://doi.org/https://doi.org/10.18637/jss.v067.i01, 2015.

Bourrier, F., Eckert, N., Nicot, F., and Darve, F.: Bayesian stochastic modeling of a spherical rock bouncing on a coarse soil, Natural Hazards and Earth System Sciences, 9, 831–846, 2009.

Breiman, L., Friedman, J., Olshen, R., and Stone, C.: Classification and regression trees. Wadsworth Int, Group, 37, 237–251, 1984.

Caduff, R., Schlunegger, F., Kos, A., and Wiesmann, A.: A review of terrestrial radar interferometry for measuring surface change in the Geosciences, Earth Surface Processes and Landforms, 40, https://doi.org/10.1002/esp.3656, 2015.

Caviezel, A., Sanchez, M., Lu, G., Christen, M., Bartelt, P., Wendeler, C., Lanter, A., et al.: Full Scale Testing of Rockfall Nets under Realistic Conditions, in: ISRM International Symposium-EUROCK 2020, International Society for Rock Mechanics and Rock Engineering, 2020.

Caviezel, A., Ringenbach, A., Demmel, S. E., Dinneen, C. E., Krebs, N., Bühler, Y., Christen, M., Meyrat, G., Stoffel, A., Hafner, E., et al.: The relevance of rock shape over mass—implications for rockfall hazard assessments, Nature communications, 12, 1–9, 2021.

Crosta, G. B., Agliardi, F., Frattini, P., and Lari, S.: Key issues in rock fall modeling, hazard and risk assessment for rockfall protection, in: Engineering geology for society and territory-volume 2, pp. 43–58, Springer, 2015.

Derron, M.-H. and Jaboyedoff, M.: Preface "LIDAR and DEM techniques for landslides monitoring and characterization", Natural Hazards and Earth System Sciences, 10, 1877–1879, https://doi.org/10.5194/nhess-10-1877-2010, 2010.

Dorren, L.: Rockyfor3D (v5.2) revealed – Transparent description of the complete 3D rockfall model, ecorisQ paper, p. 33, https://www.ecorisq.org/tool-manuals/rockyfor3d-user-manual/3-english/file, 2016.

Dorren, L., Maier, B., Putters, U., and Seijmonsbergen, A.: Combining field and modelling techniques to assess rockfall dynamics on a protection forest hillslope in the European Alps, Geomorphology, 57, 151 – 167, https://doi.org/https://doi.org/10.1016/S0169-555X(03)00100-4, 2004.

Dorren, L., Berger, F., le Hir, C., Mermin, E., and Tardif, P.: Mechanisms, effects and management implications of rockfall in forests, Forest Ecology and Management, 215, 183 – 195, https://doi.org/https://doi.org/10.1016/j.foreco.2005.05.012, 2005a.

Dorren, L., Berger, F., and Putters, U. S.: Real-size experiments and 3-D simulation of rockfall on forested and non-forested slopes, Natural Hazards and Earth System Sciences, 6, 145–153, https://doi.org/10.5194/nhess-6-145-2006, 2006.

Dorren, L. K. and Berger, F.: Stem breakage of trees and energy dissipation during rockfall impacts, Tree physiology, 26, 63–71, 2006.

Dorren, L. K., Berger, F., le Hir, C., Mermin, E., and Tardif, P.: Mechanisms, effects and management implications of rockfall in forests, Forest Ecology and Management, 215, 183–195, 2005b.

Natural Hazards and Earth System Sciences
Discussions

Eckert, N., Naaim, M., Giacona, F., Favier, P., Lavigne, A., Richard, D., Bourrier, F., and Parent, E.: Repenser les fondements du zonage règlementaire des risques en montagne «récurrents», La Houille Blanche, pp. 38–67, 2018.

Eckert, N., Mainieri, R., Bourrier, F., Giacona, F., Corona, C., Le Bidan, V., and Lescurier, A.: Une base de données événementielle du risque rocheux dans les Alpes Françaises, Revue Française de Géotechnique, p. 3, 2020.

Farmakis, I., Marinos, V., Papathanassiou, G., and Karantanellis, E.: Automated 3D jointed rock mass structural analysis and characterization using LiDAR terrestrial laser scanner for rockfall susceptibility assessment: Perissa area case (Santorini), Geotechnical and Geological Engineering, pp. 1–18, 2020.

Farvacque, M., Lopez-Saez, J., Corona, C., Toe, D., Bourrier, F., and Eckert, N.: Quantitative risk assessment in a rockfall-prone area: the case study of the Crolles municipality (Massif de la Chartreuse, French Alps), Géomorphologie: relief, processus, environnement, 25, 7–19, 2019a.

Farvacque, M., Lopez-Saez, J., Corona, C., Toe, D., Bourrier, F., and Eckert, N.: How is rockfall risk impacted by land-use and land-cover changes? Insights from the French Alps, Global and Planetary Change, 174, 138–152, 2019b.

Farvacque, M., Eckert, N., Bourrier, F., Corona, C., Lopez-Saez, J., and Toe, D.: Quantile-based individual risk measures for rockfall-prone areas, International Journal of Disaster Risk Reduction, p. 101932, 2020.

Farvacque, M., Corona, C., Lopez-Saez, J., Mainieri, R., Stoffel, M., Bourrier, F., Eckert, N., and Toe, D.: Estimating rockfall release frequency from blocks deposited in protection barriers, growth disturbances in trees, and trajectory simulations, Landslides, pp. 1–12, 2021.

Francioni, M., Antonaci, F., Sciarra, N., Robiati, C., Coggan, J., Stead, D., and Calamita, F.: Application of Unmanned Aerial Vehicle Data and Discrete Fracture Network Models for Improved Rockfall Simulations, Remote Sensing, 12, 2053, 2020.

Giacomini, A., Buzzi, O., Renard, B., and Giani, G.: Experimental studies on fragmentation of rock falls on impact with rock surfaces, International Journal of Rock Mechanics and Mining Sciences, 46, 708–715, 2009.

Guangcheng, Z., Huiming, T., Xin, X., Karakus, M., and Jiangpeng, W.: Theoretical study of rockfall impacts based on logistic curves, International Journal of Rock Mechanics and Mining Sciences, 78, 133–143, 2015.

Guerin, A., Stock, G. M., Radue, M. J., Jaboyedoff, M., Collins, B. D., Matasci, B., Avdievitch, N., and Derron, M.-H.: Quantifying 40 years of rockfall activity in Yosemite Valley with historical Structure-from-Motion photogrammetry and terrestrial laser scanning, Geomorphology, 356, 107 069, 2020.

Hantz, D., Corominas, J., Crosta, G. B., and Jaboyedoff, M.: Definitions and Concepts for Quantitative Rockfall Hazard and Risk Analysis, Geosciences, 11, https://doi.org/10.3390/geosciences11040158, 2021.

Hothorn, T., Hornik, K., Strobl, C., and Zeileis, A.: Party: a laboratory for recursive partytioning, The Comprehensive R Archive Network - Package Party, pp. 1–38, https://cran.r-project.org/web/packages/party/index.html, 2010.

Jaboyedoff, M., Dudt, J. P., and Labiouse, V.: An attempt to refine rockfall hazard zoning based on the kinetic energy, frequency and fragmentation degree, Natural Hazards and Earth System Sciences, 5, 621–632, https://doi.org/10.5194/nhess-5-621-2005, 2005.

Kanno, H., Moriguchi, S., Hayashi, S., and Terada, K.: Development of a computational design optimization method for rockfall protection embankments, Engineering Geology, p. 105920, 2020.

Kohavi, R. et al.: A study of cross-validation and bootstrap for accuracy estimation and model selection, in: Ijcai, vol. 14, pp. 1137–1145, Montreal, Canada, 1995.

Kuznetsova, A., Brockhoff, P. B., and Christensen, R. H.: lmerTest package: tests in linear mixed effects models, Journal of statistical software, 82, 1–26, 2017.

Lambert, S., Bourrier, F., and Toe, D.: Improving three-dimensional rockfall trajectory simulation codes for assessing the efficiency of protective embankments, International Journal of Rock Mechanics and Mining Sciences, 60, 26–36, 2013.

Lambert, S., Toe, D., Mentani, A., and Bourrier, F.: A meta-model-based procedure for quantifying the on-site efficiency of rockfall barriers, Rock Mechanics and Rock Engineering, pp. 1–14, 2020.

Lanfranconi, C., Sala, G., Frattini, P., Crosta, G., and Valagussa, A.: Assessing the rockfall protection efficiency of forests at the regional scale, Landslides, 17, 2703–2721, 2020.

Loye, A., Jaboyedoff, M., and Pedrazzini, A.: Identification of potential rockfall source areas at a regional scale using a DEM-based geomorphometric analysis, Natural Hazards and Earth System Sciences, 9, 1643–1653, https://doi.org/10.5194/nhess-9-1643-2009, 2009.

Lu, G., Caviezel, A., Christen, M., Demmel, S. E., Ringenbach, A., Bühler, Y., Dinneen, C. E., Gerber, W., and Bartelt, P.: Modelling rockfall impact with scarring in compactable soils, Landslides, 16, 2353–2367, 2019.

Lu, G., Ringenbach, A., Caviezel, A., Sanchez, M., Christen, M., and Bartelt, P.: Mitigation effects of trees on rockfall hazards: does rock shape matter?, Landslides, pp. 1–19, 2020.

Lundström, T., Jonsson, M. J., Volkwein, A., and Stoffel, M.: Reactions and energy absorption of trees subject to rockfall: a detailed assessment using a new experimental method, Tree Physiology, 29, 345–359, 2009.

Matas, G., Lantada, N., Corominas, J., Gili, J., Ruiz-Carulla, R., and Prades, A.: Simulation of Full-Scale Rockfall Tests with a Fragmentation Model, Geosciences, 10, 168, 2020.

Melzner, S., Rossi, M., and Guzzetti, F.: Impact of mapping strategies on rockfall frequency-size distributions, Engineering Geology, p. 105639, 2020.

Moos, C., Dorren, L., and Stoffel, M.: Quantifying the effect of forests on frequency and intensity of rockfalls, Natural Hazards and Earth System Sciences, 17, 291–304, https://doi.org/10.5194/nhess-17-291-2017, 2017.

Moos, C., Fehlmann, M., Trappmann, D., Stoffel, M., and Dorren, L.: Integrating the mitigating effect of forests into quantitative rockfall risk analysis – Two case studies in Switzerland, International Journal of Disaster Risk Reduction, 32, 55 – 74, https://doi.org/https://doi.org/10.1016/j.ijdrr.2017.09.036, advancing Ecosystems and Disaster Risk Reduction in Policy, Planning, Implementation, and Management, 2018.

Nakagawa, S. and Schielzeth, H.: A general and simple method for obtaining R2 from generalized linear mixed-effects models, Methods in ecology and evolution, 4, 133–142, 2013.

Noël, F., Cloutier, C., Jaboyedoff, M., and Locat, J.: Impact-Detection Algorithm That Uses Point Clouds as Topographic Inputs for 3D Rockfall Simulations, Geosciences, 11, 188, 2021.

Pfeiffer, T. J. and Bowen, T. D.: Computer simulation of rockfalls, Bulletin of the association of Engineering Geologists, 26, 135–146, 1989.

Pichler, B., Hellmich, C., and Mang, H. A.: Impact of rocks onto gravel design and evaluation of experiments, International Journal of Impact Engineering, 31, 559–578, 2005.

Ringenbach, A., Stihl, E., Bühler, Y., Bebi, P., Bartelt, P., Rigling, A., Christen, M., Lu, G., Stoffel, A., Kistler, M., et al.: Full scale experiments to examine the role of deadwood on rockfall dynamics in forests, Natural Hazards and Earth System Sciences Discussions, pp. 1–15, 2021.

Ruiz-Carulla, R. and Corominas, J.: Analysis of rockfalls by means of a fractal fragmentation model, Rock Mechanics and Rock Engineering, 53, 1433–1455, 2020.

Ruiz-Carulla, R., Corominas, J., and Mavrouli, O.: A methodology to obtain the block size distribution of fragmental rockfall deposits, Landslides, 12, 815–825, 2015.

https://doi.org/10.5194/nhess-2022-32
Preprint. Discussion started: 4 February 2022

Rupp, S. and Damm, B.: A national rockfall dataset as a tool for analysing the spatial and temporal rockfall occurrence in Germany, Earth Surface Processes and Landforms, 45, 1528–1538, 2020.

Saroglou, H., Berger, F., Bourrier, F., Asteriou, P., Tsiambaos, G., and Tsagkas, D.: Effect of Forest Presence on Rockfall Trajectory. An Example from Greece, in: Engineering Geology for Society and Territory - Volume 2, edited by Lollino, G., Giordan, D., Crosta, G. B., Corominas, J., Azzam, R., Wasowski, J., and Sciarra, N., pp. 1899–1903, Springer International Publishing, Cham, 2015.

Scheidl, C., Heiser, M., Vospernik, S., Lauss, E., Perzl, F., Kofler, A., Kleemayr, K., Bettella, F., Lingua, E., Garbarino, M., et al.: Assessing the protective role of alpine forests against rockfall at regional scale, European Journal of Forest Research, pp. 1–12, 2020.

Stahel, W.: Statistical regression models. Seminar for statistics, ETH Zurich, 2017.

Strobl, C., Hothorn, T., and Zeileis, A.: Party on! A New, Conditional variable-importance measure for random forests available in the party package, The R Journal, 1/2, 14–17, 2009.

Tahmasbi, S., Giacomini, A., Wendeler, C., and Buzzi, O.: Towards a novel and efficient method to determine the failure energy of rockfall chain-link meshes, Computers and Geotechnics, 119, 103 299, 2020.

Thali, U.: Schutzwirkung des Waldes anhand des Felssturz-Ereignisses «Wilerwald», Gurtnellen, vom 31. Mai 2006, Bericht Schweiz. Nationalstrassen N2, p. 21, 2009.

Volkwein, A., Schellenberg, K., Labiouse, V., Agliardi, F., Berger, F., Bourrier, F., Dorren, L., Gerber, W., and Jaboyedoff, M.: Rockfall characterisation and structural protection - a review, Natural Hazards and Earth System Sciences, 11, 2617–2651, https://doi.org/10.5194/nhess-11-2617-2011, 2011.

Von Neumann, J. and Ulam, S.: Monte carlo method, National Bureau of Standards Applied Mathematics Series, 12, 36, 1951.

Wang, B. and Cavers, D. S.: A simplified approach for rockfall ground penetration and impact stress calculations, Landslides, 5, 305, 2008.

Yan, P., Zhang, J., Kong, X., and Fang, Q.: Numerical simulation of rockfall trajectory with consideration of arbitrary shapes of falling rocks and terrain, Computers and Geotechnics, 122, 103 511, 2020.

Yang, J., Rahardja, S., and Fränti, P.: Outlier detection: how to threshold outlier scores?, in: Proceedings of the International Conference on Artificial Intelligence, Information Processing and Cloud Computing, pp. 1–6, 2019.

https://doi.org/10.5194/nhess-2022-32
Preprint. Discussion started: 4 February 2022

Natural Hazards and Earth System Sciences
Open Access
Discussions

Table 1. Characteristics of the 18 study sites with mapped SW used in this study. $Site$ provides the site name, which are abbreviated with the first 5 letters throughout the article, as well as the country (AT = Austria, CH = Switzerland, FR = France, GR = Greece, IT = Italy) and a sequential site number per country; H_c refers to the total cliff height (rockfall release or source area); ϕ_{Tr} is the mean slope angle in the transit area; S_Type refers to the complexity of the topography explained in Fig. 2; $\overline{L_{Tr}}$ is the average length of the transit slope; G is the mean basal area in the forest between the SW and the foot of the cliff; n represents the number of mapped SW; SW_{vol} is the volume range of the mapped SW; SW_{des} described which SW we mapped in the field (1 = all blocks of one specific recent rockfall event, 2 = all blocks from multiple recent events, 3 = selected blocks (for explanation see text) of one specific recent rockfall event, 4 = selected blocks from multiple recent events).

$Site$	$Rocktype$	$Lat(°)$	$Long(°)$	$H_c(m)$	$\phi_{Tr}(°)$	$SType$	$\overline{L_{Tr}}(m)$	$G(m^2/ha)$	n	$SW_{vol}(m^3)$	SW_{des}
Bottingen (CH1)	Limestone	46.698	8.249	400	33	3	390	31	2	0.3-7.5	4
Claro (CH2)	Granite	46.262	9.025	60	23	3	65	28	52	0.03-10	2
Crolles (FR1)	Limestone	45.285	5.865	350	30	2	685	39	7	1-30	4
Evolène (CH3)	Calcschist	46.106	7.474	50	29	3	1750	49	2	180/200	3
Flaesch (CH4)	Limestone	47.030	9.519	50	29	2	285	29	98	0.02-4	2
Greece (GR1)	Limestone	38.582	22.665	150	28	2	330	24	61	0.01-38	2
Gsteigwiler (CH5)	Limestone	46.652	7.886	500	30	3	205	25	26	0.9-6	4
Gurtnellen (CH6)	Granite	46.730	8.631	50	33	3	835	35	13	8-50	3
Kilknerwald (AT1)	Amphibolite	46.986	10.034	120	31	3	300	55	6	0.5-8	4
Orvin (CH7)	Limestone	47.165	7.210	100	28	1	635	49	198	0.04-5	2
Schmitten (CH8)	Dolomite	46.691	9.679	70	31	2	440	26	45	0.05-0.8	2
St.Imier (CH9)	Limestone	47.154	6.991	20	30	1	365	24	47	0.01-2.7	4
Taesch (CH10)	Gneiss	46.081	7.789	30	30	3	475	29	176	0.05-50	1
Tramin (IT1)	Limestone	46.324	11.229	50	29	2	520	12	9	0.6-72	3
Varces (FR2)	Limestone	45.083	5.653	400	33	3	910	23	11	4-33	3
Varces2 (FR3)	Limestone	45.081	5.644	50	27	2	295	22	6	1.3-12	4
Vaujany (FR4)	Granite-Gneiss	45.202	6.049	0	34	1	190	32	9	0.4-0.9	3
Veyrier (FR5)	Limestone	45.875	6.188	120	26	2	350	26	1	6.3	3